Energy Conversion and Management: X 28 (2025) 101257

Contents lists available at ScienceDirect

Energy Conversion and Management: X

journal homepage: www.sciencedirect.com/journal/energy-conversion-and-management-x

Methodology for the use of aerial thermography as a validation method for outdoor thermal comfort simulations☆

V.P. Lopez-Cabeza *, M. Videras-Rodriguez, S. Gomez-Melgar, J.M. Andujar-Marquez

Research Centre for Technology, Energy and Sustainability (CITES), Universidad de Huelva, Huelva, Spain

ARTICLE INFO

Keywords:
Aerial thermography
Mean radiant temperature
Urban thermal comfort
Urban microclimate simulation

ABSTRACT

The urban heat island (UHI) effect underscores the importance of outdoor spaces in urban planning and design, where thermal comfort has become a critical consideration. Mean Radiant Temperature (MRT) is a dominant factor influencing human thermal perception, making its accurate simulation essential for creating comfortable urban environments. Despite the widespread use of simulation tools, a significant gap exists in their validation, particularly during early design stages. This study introduces a novel methodology for calibrating and validating longwave MRT simulations using aerial thermography, providing a practical and robust approach to improving simulation accuracy. As an example of the proposed methodology, a practical application is carried out using Ladybug Tools® (LBT), a widely used simulation tool known for its powerful features, open access, and integration with early-stage design workflows. It was used to simulate an open space located in Huelva, Spain, under summer conditions. The calibration process refines parameters such as albedo, shading, and grid resolution, ensuring results align with ASHRAE guidelines. The findings demonstrate that, after calibration, LBT can effectively predict MRT, with minor discrepancies attributed to inherent model limitations. This study highlights the potential of aerial thermography to enhance the reliability of MRT simulations across diverse platforms, providing urban planners and designers with a valuable framework for assessing thermal comfort. By bridging a critical validation gap, this work supports the development of more sustainable and thermally comfortable urban spaces, paving the way for broader applications in urban planning and climate adaptation strategies.

1. Introduction

The current climate crisis is affecting the local climate in our cities. The so-called Urban Heat Island (UHI) effect, defined as the higher temperatures that are found in city areas compared to surrounding rural ones, is also being exacerbated by climate change [1]. This makes outdoor spaces in cities even less livable, especially in extremely hot weather. In this sense, the design and planning of outdoor spaces are critical in order to mitigate the effects of UHI [2].

Research in recent years has focused on improving outdoor thermal comfort in cities, as a parameter that is related to the use of outdoor areas. If people feel no stress related to temperature, it is more likely that they will stay longer and more often in a public space. Thermal comfort is not only related to air temperature. Many factors intervene in the state of mind called thermal comfort [3]: there are factors related to the person (physical and mental factors, which are not under outside control), and factors related to the environment. These are air temperature, wind speed, radiant temperature, and humidity. These factors will affect the radiant exchange between the body and the environment, affecting the person's sensation. Other factors not directly related to the climatic environment, such as noise, pollution, or aesthetics in the urban settings, may also affect the thermal perception of the person [4]. Different indices have been developed to measure thermal comfort, such as the Universal Thermal Climate Index (UTCI) [5], Physiological Equivalent Temperature (PET) [6], and Standard Effective Temperature (SET) [7], all of which consider the previously described personal and environmental factors.

Among the environmental factors, MRT has been consistently identified as the most influential parameter in outdoor thermal comfort, particularly under high solar radiation and low wind conditions typical of warm climates [8]. The MRT is a parameter that expresses the effects of complex radiant environments in one temperature-dimension index, including both long-wave and short-wave radiation. This means that it accounts for the direct and diffuse solar radiations, and the thermal radiation from the surfaces surrounding the observer, including the sky.

☆ This article is part of a special issue entitled: 'SDEWES 2024_ECMX' published in Energy Conversion and Management: X.

* Corresponding author.
E-mail address: victoria.lopez@pi.uhu.es (V.P. Lopez-Cabeza).

https://doi.org/10.1016/j.ecmx.2025.101257
Received 3 January 2025; Received in revised form 25 August 2025; Accepted 8 September 2025
Available online 11 September 2025

Nomenclature

UHI	Urban Heat Island effect
MRT	Mean Radiant Temperature
LW MRT	Longwave Mean Radiant Temperature
SW MRT	Shortwave Mean Radiant Temperature
SDIM	Six Direction Integral method (for MRT calculations)
LBT	Ladybug Tools® (simulation software)
UAV	Unmanned Aerial Vehicle
σ	Stephan- Boltzman constant (5.67E-8 W/m^2K^4
K_i	Shortwave radiation
F_i	View factors from each surface to the user
ε	Emissivity
E_i	Longwave radiation
LW_{delta}	Longwave delta, including the sky
T_{sky}	Sky temperature
T_a	Air temperature
ERF_{solar}	Solar Effective Radiant Field
f_{eff}	Fraction of the body that can radiate heat (related to posture)
f_{bes}	Fraction of body exposed to direct solar radiation
I_{diff}	Diffuse radiation
I_{th}	Global horizontal radiation
I_{dir}	Direct solar radiation
R_{floor}	Ground reflectance or albedo
UTCI	Universal Thermal Climate Index
RMSE	Root mean square error
MAPE	Mean absolute percentage error
R^2	Coefficient of Determination
cvRMSE	Coefficient of variation of the Root Mean Square Error
nMBE	Normalized Mean Bias Error

Previous literature has identified MRT as the most influential parameter on outdoor thermal comfort, with a strong correlation with thermal comfort indexes [9,10]. In urban settings with moderate humidity and limited air movement, such as the Mediterranean climate of the coastal urban areas of Spain, MRT tends to be determinant on thermal perception over the other climatic parameters [11,12]. Additionally, MRT exhibits strong spatial and temporal variability, as it is highly sensitive to urban geometry, materials, shading, and sky exposure [13]. This makes it both crucial for design decisions and challenging to measure in situ, especially across large or complex urban areas.

Commonly used methods to assess in situ MRT include the use of globe thermometers, net radiometers, and thermography [14]. The globe thermometer is a black or grey sphere-shaped tool with an internal bulb thermometer that estimates the MRT by considering the temperature of the globe, its characteristics, and climatic data such as air temperature and wind speed. This method is common and practical [15], although previous research has stated that it can overestimate MRT because of its greater shortwave absorptance compared to a person and because the standing posture is represented by a sphere [10], and the long response time of the instrument [16]. A net radiometer is a tool consisting of a mobile shaft containing sensors such as pyrgeometers and pyranometers, measuring respectively short and long wave radiation. These tools can be used following different methodologies, measuring the radiation from different directions, in order to accurately measure the net radiation that would be received by a body. The six directions integral method (SDIM) is considered the most accurate, although other methods exist, given the complexity of measuring six directions in space [17]. The use of net radiometers is considered the most accurate and fastest, although it is not commonly used because it is costly and difficult to implement in large-scale settings [18]. In addition, instruments such as globe thermometers or net radiometers provide point-based measurements that may not capture the full heterogeneity of the urban environment. In this sense, infrared thermography, following the Stefan-Boltzmann law, allows the measurement of longwave radiation in larger areas by converting surface temperatures into radiation weighted by view factors [19].

Recent studies have focused on the use of remote sensing technologies to measure MRT. Satellite data, one type of remote sensing, combined with weather stations' information, is useful for studying the UHI effect and vegetation influence [20]. However, the lack of temporal and spatial resolution makes it unsuitable for small-scale case studies. This is overcome with the use of another remote sensing technique, aerial thermography, which can be used to measure surface temperatures and allows the calculation of MRT [21]. Aerial thermography is a versatile method that facilitates the measurement of surface temperatures of pavements and facades in a public space in a single experiment, saving time for operators and ensuring their safety [22]. Aerial thermography has been evaluated by the scientific community for the measurement of surface temperatures in urban spaces and has demonstrated advantages over satellite acquisition methods [23]. In terms of MRT calculation, aerial thermography simplifies the in-situ acquisition of thermal images compared to the use of hand-held thermal cameras [24], as it allows capturing a larger dimension of the terrain from a nadir perspective and simultaneously measuring surface temperatures in a single image [25].

In the field of urban planning, developing and validating reliable simulation methods for MRT is essential, not only because of its central role in comfort, but also due to the practical difficulty of measuring it directly in real-world urban contexts. As noted in several review studies [14,26,27], the reliability of thermal comfort simulations is highly dependent on calibration and validation, especially for complex variables such as MRT, which are sensitive to local geometry, material properties, and sky conditions. Lack of validation can lead to significant deviations in key thermal indicators, which in turn may compromise urban design decisions. As previous work has demonstrated, discrepancies between predicted and observed values can be substantial if simulations are based solely on default parameters or weather file data without local calibration [13]. Even well-established tools like ENVI-met and RayMan can produce diverging results if not properly calibrated [28].

In urban microclimate modelling, calibration involves adjusting model parameters to ensure that simulations accurately reflect observed conditions [13]. This can be done manually by tuning key variables such as surface albedo, emissivity, or roughness length, or through automated optimization techniques like genetic algorithms, Monte Carlo simulations, or Bayesian calibration [29]. A common preliminary step is sensitivity analysis, which identifies the most influential parameters to prioritize during calibration. Once calibrated, the model undergoes validation to assess its performance under different conditions or locations. Among the validation techniques, the most commonly used are comparing modelled outputs, such as air temperature, mean radiant temperature, wind speed, or thermal comfort indices, against field measurements from weather stations, mobile sensors, or infrared thermography, comparison between models that use the same forcing and domain, a statistical assessment of model performance with indicators such as RMSE, MAE, bias error, and R^2, and a sensitivity analysis of model input parameters [30]. The validation should comprise temporal and spatial resolution to ensure model accuracy.

In the field of simulation, the progress in computational resources and tools has significantly enhanced our ability to forecast the performance of outdoor spaces. This advancement empowers us with information before designing outdoor environments, facilitating the identification of optimal design solutions. For the assessment of MRT by

computer simulation, there are many computer tools such as ENVI-met® [31], RayMan® [32] or SOLWEIG® [33], validated by the scientific community by testing in situ measurements and simulations for the calculation of MRT [34], and specifically in outdoor environments [15]. ENVI-met® is considered the best suited for outdoor microclimate studies [27,35] since it incorporates computational fluid dynamics (CFD) simulation, although this reduces its suitability for the early design process. As an alternative, among the different simulation tools available, one of the best suited for early design is the Ladybug Tools® (LBT) [36]. They are a set of plugins for Grasshopper®, the parametric modeling tool for the CAD software Rhinoceros®, that links the geometric model with several simulation engines in order to predict different parameters. All these engines are open source, with the advantages that this involves. In addition, the communication between all the tools and the model allows for addressing changes easily and in an informed way.

LBT has previously demonstrated its capability to accurately predict microclimate conditions in semi-outdoor spaces such as inner courtyards of buildings, providing valuable insights for early design stages [37]. Previous studies validate its use to analyze outdoor thermal comfort, contrasting with ENVI-met® simulations [38]. However, some other studies showed discrepancies between the MRT predicted by this and other software [39]. Most of the studies use the legacy version of the software, and there are only a few studies using the current version of the software, which has undergone major development recently. Given the importance of the MRT parameter on outdoor thermal comfort, this gap should be overcome in order to validate the use of this tool in the design of outdoor spaces. Despite the large number of studies using LBT to predict outdoor microclimate, this number is lower considering only studies that validate the results with monitored data. Among the studies that validate the results, even less focus on MRT. This is a consequence of the difficulties that the measurement of MRT involves. A previous study using LBT to validate it in MRT prediction under the shade validated it using monitoring data from net radiometers and SDIM and found that longwave radiation was overestimated in the simulation [40]. However, the experiment in this study was isolated from a real urban setting, where other parameters such as surrounding buildings reflections may have an important influence on the results.

Considering the gaps identified in the literature (the scarcity of validation studies for simulation tools to estimate MRT in real urban environments, the measurement difficulties, and the untapped potential of aerial thermography for this purpose), this study proposes a methodology for validating simulated MRT using UAV-based thermal imaging as reference data. The comparatively under-validated Ladybug Tools® software is used as the case-study platform, both for its versatility in early design workflows and for its explicit calculation of the longwave MRT component, which aligns with the thermography-based validation approach. The proposed methodology is applied to a pedestrian area in Huelva (Spain), a subtropical coastal city, during a typical summer day. The workflow involves aerial thermal data acquisition, simulation of the same area in LBT, and statistical validation of simulated versus observed MRT. By combining high-resolution remote sensing with open-source simulation, this study not only benchmarks LBT's performance in a real-world context but also delivers a transferable validation framework that can be applied to other tools and settings. This contributes to more reliable MRT modelling in urban climate studies, ultimately supporting the design of outdoor spaces with improved thermal comfort and resilience to UHI effects [41].

2. Materials and methods

2.1. Developed methodology

This study introduces a novel methodology for validating Mean Radiant Temperature (MRT) simulations, with a focus on enhancing their applicability to outdoor thermal comfort studies. The methodology comprises five stages. In the first stage, monitoring data is collected through aerial thermography, following established protocols [21], to construct a 3D surface temperature model. Concurrently, data from local weather stations and the target simulation model are gathered. The second stage involves setting up the simulation model and calibrating the initial results by comparing simulated and observed surface temperatures, followed by longwave MRT. Calibration adheres to ASHRAE recommendations for energy simulations [42]. In the third stage, MRT is calculated from the monitoring data, combining aerial thermography for longwave MRT and weather station data for shortwave MRT using the SDIM method. The fourth stage focuses on validating the simulation model against ASHRAE thresholds. Finally, in the fifth stage, the validated model is employed to simulate outdoor thermal comfort indices with greater accuracy. This workflow is diagrammed in Fig. 1. This innovative approach provides a standardized, replicable framework for improving the reliability of MRT simulations, enabling more precise assessments of outdoor thermal comfort and informing better design and policy decisions for urban environments.

In order to test the previous methodology, a case study approach is employed, contrasting MRT values derived from field data with those obtained through simulation, which in this specific case will be carried out using LBT. Once validated, the simulation model is used to analyze thermal comfort at different times of the day. This research highlights the workflow, examines the sources of discrepancies, and discusses potential improvements, offering a robust framework for enhancing the accuracy of MRT simulations across diverse tools and scenarios.

2.2. Case study area

The methodology described in the previous sections was applied in a case study approach, an urban square in the historic center of Huelva, in the south of Spain (37.2620° N, 6.9427° W, 54 asl). The climate in this city is classified as Csa according to the Koppen-Geiger classification [43], meaning mild winters and hot and dry summers. The characteristics of this climate make it interesting to analyze urban areas in the summer months to examine thermal comfort under hot conditions and improve it to enhance users' experience.

The selected square is a historic square representing this kind of space in the Mediterranean cities. Its dimensions are 45 m long and 25 m wide for pedestrians and surrounded by four traffic roads, meaning a total of 2100 m^2. It is surrounded by buildings of two to four floors and to the west there is a high church (Fig. 2). The pavement of the square is mainly hard, consisting of granite tiles and pebbles. Around the pedestrian area, there are some vegetation pits where palm trees grow and provide some shade to around 15 % of the square. The material properties covering the floor of the square are summarized in Table 2.

2.3. Data acquisition

The monitoring data for this study is obtained from a previous publication [21]. The data acquisition took place at three different times on the 20th of July 2021 (11.00, 15.00, and 19.00 h), corresponding to three different positions of the sun. An aerial survey was carried out with a UAV equipped with a thermal and RGB camera to measure surface temperatures needed to calculate the LW MRT. Permissions from AESA, the Ministry of the Interior, and the local City Council, were obtained in order to perform the flight. All the legal requirements were complied with, such as the registration of the operator, pilot, and UAV. The drone weighed less than 10 kg, included safety items, and the flight complied with regulations on altitude, visual line of sight, and safety distances. The area was cordoned off to ensure public safety. Given the operational constraints and to optimize the process, the decision was made to focus the monitoring on a single day. Some information about the instruments used is presented in Table 1. In addition, weather data for that day was obtained from a nearby official meteorological station (5 km from the case study area). This climatic data was inserted in the EPW file

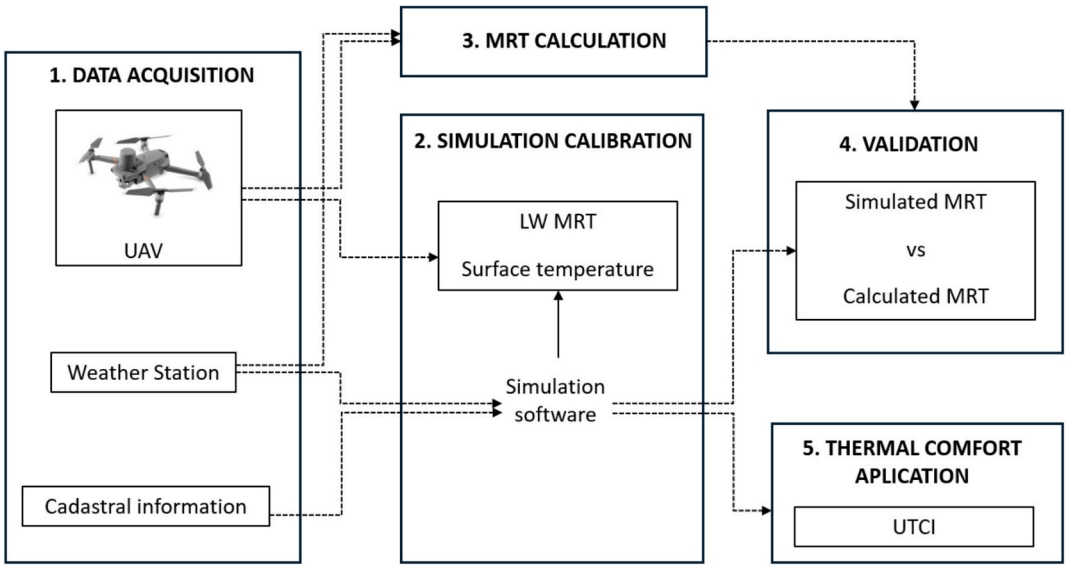

Fig. 1. Methodology workflow.

Fig. 2. Location of the case study area. Up: Aerial view of the city center of Huelva. Down left: Aerial view of the square. Down right: Details of the square: The statue in the center and the church at the back of the image.

(EnergyPlus® Weather format) used by the simulation software, and it is represented in Fig. 3. More information about the monitoring process can be found in the referenced publication.

2.4. Mean radiant temperature calculation

MRT calculation in the outdoor environment follows Hope's equation (Eq. (1)), where it is derived from the longwave and shortwave radiation received by a human body [44]:

$$MRT = \sqrt[4]{\frac{1}{\varepsilon_p \sigma}\sum_{i=1}^{n}\left(\varepsilon_p E_i + \alpha_k K_i\right)F_i} - 273.15, \quad (1)$$

where K_i is the incident shortwave radiation (W/m^2), E_i is the longwave radiation (W/m^2), σ is the Stefan-Boltzmann constant (5.67E-8 W/m^2 K^4), F_i are the view factors from each surface to the user, α_k is the

Table 1
Materials and characteristics of the ground.

Material	Coverage Percentage (%)	Use	Albedo
Granite tiles	16.5	Pedestrian area	0.50
Pebble stone	17.2	Pedestrian area	0.35
Terrazzo tiles	7.5	Sidewalks	0.20
Cobblestone road	46.8	Traffic roads	0.15
Dirt soil	12.0	Vegetation pit	0.20

Table 2
Measuring instrument specifications.

Measuring instrument	Model	Specifications
Thermal camera	Testo 875 1i	Spectral band: 8—14 μm Thermal sensitivity: < 50 mK IR Resolution: 160 × 120 pixels Lens: HQ 32° x 23° with manual focus Measuring range: − 30 °C − 350 °C
Thermohygrometer	RS-91 Pro	Humidity range: 0.0—100.0 % Temperature range: 20.0 °C − 60.0 °C Humidity Resolution: 0.1 % Temperature Resolution: 0.1 °C
UAV	DJI Mavic 2 Enterprise Advanced	Takeoff Weight (without accessories): 909 g Dimensions: 322 × 242 × 84 mm (unfolded) Max speed: 72 km/h Spectral band: 8—14 μm Thermal sensor resolution: 640 × 512 pixels Measuring range: − 40 °C − 550 °C Digital zoom: 32x digital zoom, 16x thermal zoom

shortwave absorption coefficient (0.7) and ε_p is the emissivity of the skin (0.97).

Using aerial thermography, the temperatures from surrounding surfaces can be easily measured. From them, the longwave radiation, E_i, is computed using the following equation (2) [45]:

$$E_i = \varepsilon_i \sigma (273.15 + T_i)^4, \quad (2)$$

where T_i is the temperature of the surrounding surfaces, and ε_i their emissivity. The sky was supposed to be at the same temperature as the air, and its emissivity was computed as a function of specific humidity in the air [46]. With this data, LW MRT can be calculated using Eq. (1) considering only the longwave radiation, and obtaining the view factors from each surface through the procedure described in the referenced publication:

$$LWMRT = \sqrt[4]{\frac{1}{\sigma}\sum_{i=1}^{n}(E_i)F_i} - 273.15 \quad (3)$$

In this study, there was no in situ measurement of shortwave radiation, aiming to propose a methodology based solely on remotely obtained data. For that reason, the calculation of the shortwave radiation was based on the solar radiation information from the weather station (direct and diffuse). The conversion of this data to in situ data was achieved using simulation in Ladybug Tools® and the six directions integral method (SDIM) to obtain the shortwave radiation on a person. The SDIM considers the human body as a prism with different view factors, which are 0.06 for the radiation from above and below and 0.22 for horizontal directions. It is considered the most accurate method for outdoor studies [47]. Once LW and SW radiations are obtained, MRT is derived following Eq. (1).

2.5. MRT simulation

Ladybug Tools® (LBT) [48] was used in this study primarily as a case study to apply and test the proposed methodology for validating simulated longwave MRT using aerial thermography as reference data. While LBT is increasingly adopted in urban and architectural design workflows, it remains under-validated in outdoor comfort applications, particularly regarding MRT simulation accuracy. LBT was selected in this research for several reasons. Unlike tools such as ENVI-met®, which provide detailed CFD-based microclimate modeling but involve complex setup and long computation times, LBT offers a more agile and transparent workflow, allowing fast iteration and adjustment of boundary conditions, surface properties, and urban geometry. Moreover, it is one of the few simulation tools that explicitly outputs the longwave component of MRT, which makes it especially compatible with validation methods based on aerial thermography. As an open-source, parametric, and flexible platform integrated with Rhinoceros® and Grasshopper®, LBT supports rapid simulation-feedback loops that are valuable during the early stages of urban design. However, despite its popularity and ease of use, the current version of LBT has undergone substantial development and still lacks comprehensive scientific validation, especially in outdoor thermal comfort studies.

The model is built in Rhinoceros based on the geometrical information from the square. Then it is linked to a script in Grasshopper. The components from Ladybug Tools® allow us to set up the energy model, which is calculated using EnergyPlus engine [49], and the radiation model, which is simulated using Radiance [50]. All these simulation engines are controlled within the interface of Grasshopper through LBT components, allowing a fast and versatile process to visualize and

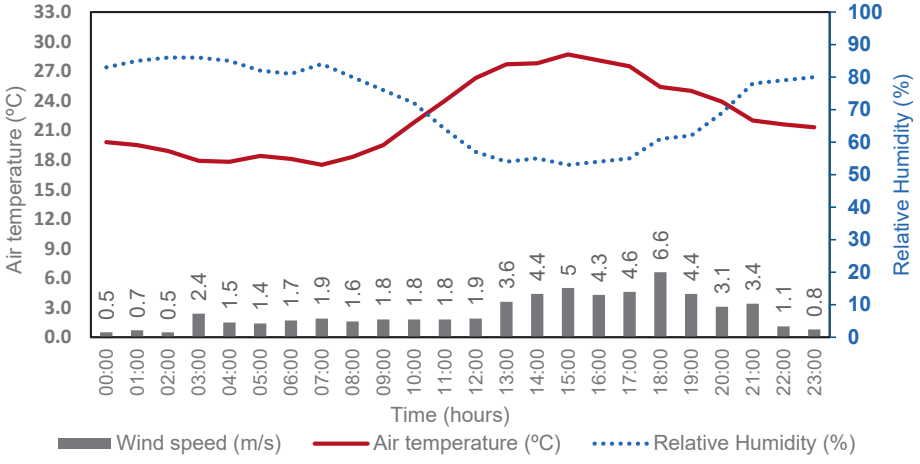

Fig. 3. Weather data from the official station on the 20th of July 2021.

analyze the results. The version used in this study is LBT 1.8.

The LBT "UTCI Comfort Map" component is prepared to perform thermal comfort calculations that also provide the mean radiant temperature results [51]. The MRT (Eq. (4)) is composed of longwave components (LW MRT and LW_{delta}, this last one specifically for the outdoors, as it includes heat exchange with the sky) using EnergyPlus methods [49] and shortwave component, SW MRT, derived from the ASHRAE SolarCal method [52].

$$MRT = LW\,MRT + LW_{delta} + SW\,MRT \tag{4}$$

The longwave mean radiant temperature is calculated using Eq. (5):

$$LW\,MRT = \sqrt[4]{\sum_{i=1}^{n}\left(F_i T_i^4\right)} - 273.15, \tag{5}$$

where T_i is the temperature of each surface [K] and F_i are the view factors to each surface. On the other hand, the longwave delta is calculated using Eq. (6):

$$LW_{delta} = 0.5{*}f_{svv}{*}(T_{sky} - T_a) - 273.15, \tag{6}$$

where f_{svv} is the view factor calculated using HB View Factor Component and T_{sky} and T_a are the sky and air temperatures from the EPW weather file. Longwave radiant temperatures are obtained by computing spherical view factors from each sensor to the surfaces of the model using Radiance engine. These view factors are then multiplied by the surface temperatures output by EnergyPlus to yield longwave MRT at each sensor. To account for sky radiant exchange, each sensor's sky view is multiplied by the EPW sky temperature.

A Radiance-based enhanced 2-phase method is used for all shortwave MRT calculations, which precisely represents direct and diffuse radiation by tracing a ray from each sensor to the solar position and considering the reflected component from the surroundings. The model follows the SolarCal (Eq. (7)) to derive the Solar Effective Radiant Field (ERF_{solar}) from which SW MRT can be obtained:

$$ERF_{solar} = \left(0.5 f_{eff} f_{svv}\left(I_{diff} + I_{th} R_{floor}\right) + \frac{A_p f_{bes} I_{dir}}{A_D}\right)\frac{T_{sol}\alpha_k}{\varepsilon_p}, \tag{7}$$

where f_{eff} is the fraction of the body that can radiate heat (related to posture), f_{svv} is the sky view factor, f_{bes} is fraction of body exposed to direct solar radiation, I_{diff} is the diffuse radiation [W/m^2], I_{th} is the global horizontal radiation [W/m^2], I_{dir} is the direct radiation [W/m^2], R_{floor} is ground reflectance or albedo, and A_p / A_D is the projection factor determined through a look up table available at ASHRAE and is determined by solar altitude, solar azimuth and the body's related angle.

The outputs of the "UTCI Comfort Map" component include UTCI and some of the related parameters such as MRT, LW MRT, and SW MRT delta, which are used in this study. The monitored climatic parameters were used to morph the weather file in order to simulate the same day. The workflow used in LBT is diagramed in Fig. 4:

2.6. Modeling and simulation set up

The simulation set up has three steps: Constructing the geometrical model, setting up the boundary conditions and transforming the geometry into a LBT model that includes material properties to perform the simulations.

2.6.1. Geometry modelling

Information to build the geometry model in Rhinoceros was obtained from different sources, from cadastral information (dimensions of the square and buildings around) to aerial images to identify materials and distribution of vegetation. The model was constructed using one solid per floor for each building, as recommended for urban energy simulations. However, the geometry for the ground had to be carefully modeled, building one solid per material and splitting the upper surface into grid faces, following the geometry, to gain accuracy. These faces were up to 2 by 2 m to ensure enough accuracy. Regarding the vegetation, it was modeled with prisms with a similar size of the tree canopy, as this is the way to include them in the simulation, although it can be considered a very limited approximation of the real tree geometry. The geometry model of the square is shown in Fig. 5.

2.6.2. Boundary conditions

LBT utilizes an EnergyPlus (EPW) weather file to define the boundary conditions for simulations. The appropriate EPW file for the city of Huelva was obtained from Climate.OneBuilding.Org [53]. The hourly data of air temperature, relative humidity, wind speed, direct solar radiation and diffuse solar radiation from the official weather station replaced the original EPW data for the day under analysis. Incorporating on-site meteorological measurements enabled precise calibration of boundary conditions for the simulations, minimizing variables that could account for discrepancies between observed and simulated outcomes.

2.6.3. LBT model

The geometry built in Rhinoceros is imported to Grasshopper to transform it into an energy model in LBT. In this stage, material properties are defined, as well as other simulation specifications needed for

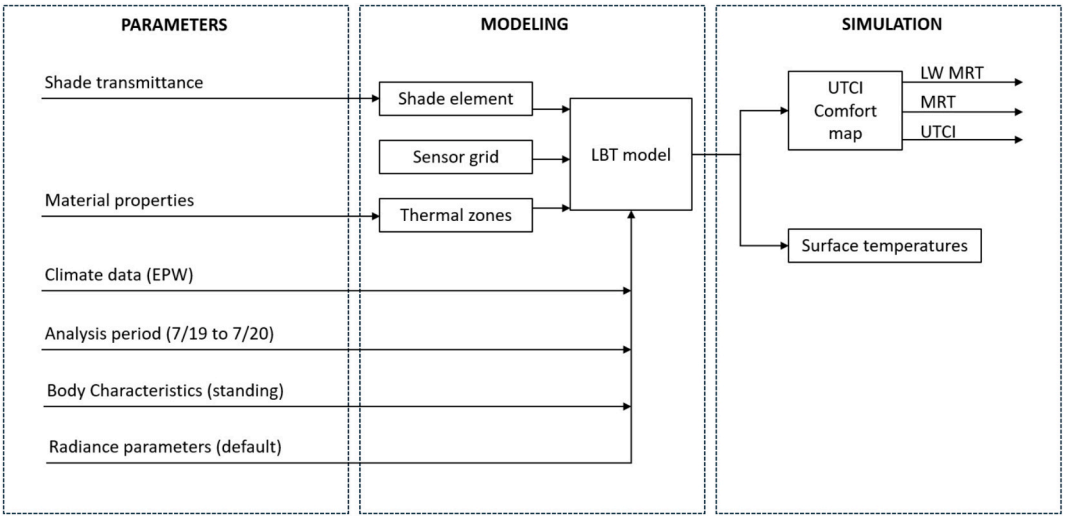

Fig. 4. LBT simulation workflow.

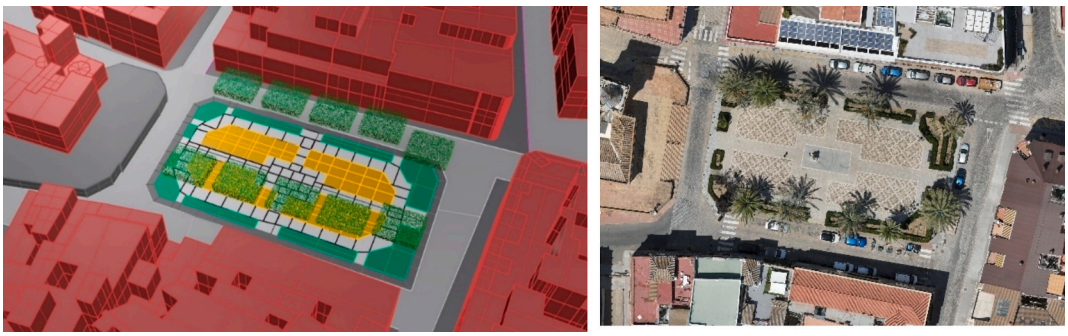

Fig. 5. Left: Image of the model for the simulation. Right: Aerial view of the square.

the energy simulation, such as programs for the buildings (residential) or context elements. The specifications of the materials were used to create custom materials in the software to accurately predict their performance (Table 3). It is needed to mention that the vegetation was considered as a context shade with 0.7 transparency, and not its evapotranspiration effect, since LBT is not able to simulate that, considering this one of the limitations of the software.

2.7. Performance parameters

In order to calibrate the simulations, the parameters that were compared to the monitoring were surface temperature and longwave mean radiant temperature at the times of monitoring (11.00, 15.00, and 19.00 h) on the 20th of July 2021. The surface temperatures were obtained in two profiles of the squares, following the longitudinal and transversal middle sections of the square as shown in Fig. 6a. Longwave Mean Radiant Temperature results were calculated at 20 fictitious points at 1.5 m above the ground in the square, as shown in Fig. 6b. The same points were simulated to compare the results.

The accuracy between the simulation and measured results was analyzed following diverse criteria. Given the lack of a standardized methodology to evaluate the accuracy of this kind of simulation, the ASHRAE Guidelines recommendations for energy model calibrations were used [42]. This standard proposes using the coefficient of determination R^2, the coefficient of variation of the Root Mean Square Error (cvRMSE), and the normalized Mean Bias Error (nMBE). These parameters follow Eqs. (8), (9) and (10):

$$R^2 = \frac{\sum_{i=1}^{n}(O_i - \overline{O}_i)(P_i - \overline{P}_i)}{\left[\sum_{i=1}^{n}(O_i - \overline{O}_i)^2 \sum_{i=1}^{n}(P_i - \overline{P}_i)^2\right]^{1/2}} \tag{8}$$

$$cvRMSE = \frac{1}{\overline{O}}\left(\frac{\sum_{i=1}^{n}(P_i - O_i)^2}{n-1}\right)^{1/2} \tag{9}$$

$$nMBE = \frac{\sum_{i=1}^{n}(O_i - P_i)}{(n-1)\overline{O}} \tag{10}$$

where P_i is the forecast from the simulation method, O_i is the actual value at the monitoring, $\overline{O}$ is the mean of the monitoring values, $\overline{P}_i$ is the mean of the forecasted values, and n is the number of samples.

These guidelines state that, for hourly data collection intervals, the R^2 value should be over 0.75, cvRMSE under 30 % and nMBE under ± 10 %. In addition, the Mean Absolute Percentage Error (MAPE) and the Root Mean Square Error (RMSE) were also performed following previous research recommendations [54], using Eqs. (11) and (12) [55]:

$$RMSE = \left(\frac{\sum_{i=1}^{n}(P_i - O_i)^2}{n}\right)^{1/2} \tag{11}$$

$$MAPE = \frac{1}{n}\sum_{i=1}^{n}\left|\frac{O_i - P_i}{O_i}\right| x100 \tag{12}$$

3. Results

This section presents the results obtained from the simulations and compares them with monitoring data. The simulations underwent a calibration process by adjusting parameters to achieve the precision required by ASHRAE standards. First, the results for surface temperature are discussed. Next, the calibrated longwave MRT results are presented, which serve as the basis for validating the simulation methodology. The third section compares the MRT derived from monitoring data with the MRT from the simulation to ensure methodological accuracy. Finally, the results of the thermal comfort simulations are provided, demonstrating the potential of the software for improving urban thermal environments.

3.1. Surface temperature results

The two temperature profile lines are shown, West-East (Fig. 7) and North-South (Fig. 8), comparing monitored thermal values and simulated ones on the ground surface. The mean values of monitored surface temperature were 27.0 °C, 43.1 °C and 37.4 °C while the simulated ones were 29.5 °C, 43.6 °C and 40.8 °C. They showed good accuracy at 15:00 h and relatively higher values in the simulation than monitoring ones at morning and evening hours. Furthermore, the monitoring data showed faster variations in temperature due to material changes and shades, as it can be seen in the dotted lines, which cooled down faster in the limits of the square (building shade) or in the shade in the middle produced by the statue. The North-South profile (Fig. 8) shows greater variations due to shadings from vegetation, as it crosses the two lines of palm trees in

Table 3
Material properties used in the simulation.

Material	Density (kg/m^3)	Thermal conduct. (W/mK)	Specific Heat capacity (J/kgK)	Thermal absorptance	Solar absorptance
Granite tiles	2750	3.10	852	0.96	0.35
Pebble	2400	1.63	868	0.96	0.35
Cobblestone	2750	3.10	852	0.90	0.25
Dirt soil	1100	0.35	1200	0.90	0.30
Cement render	1860	0.72	840	0.90	0.70

Fig. 6. a) Profile lines and b) points for the analysis of the results.

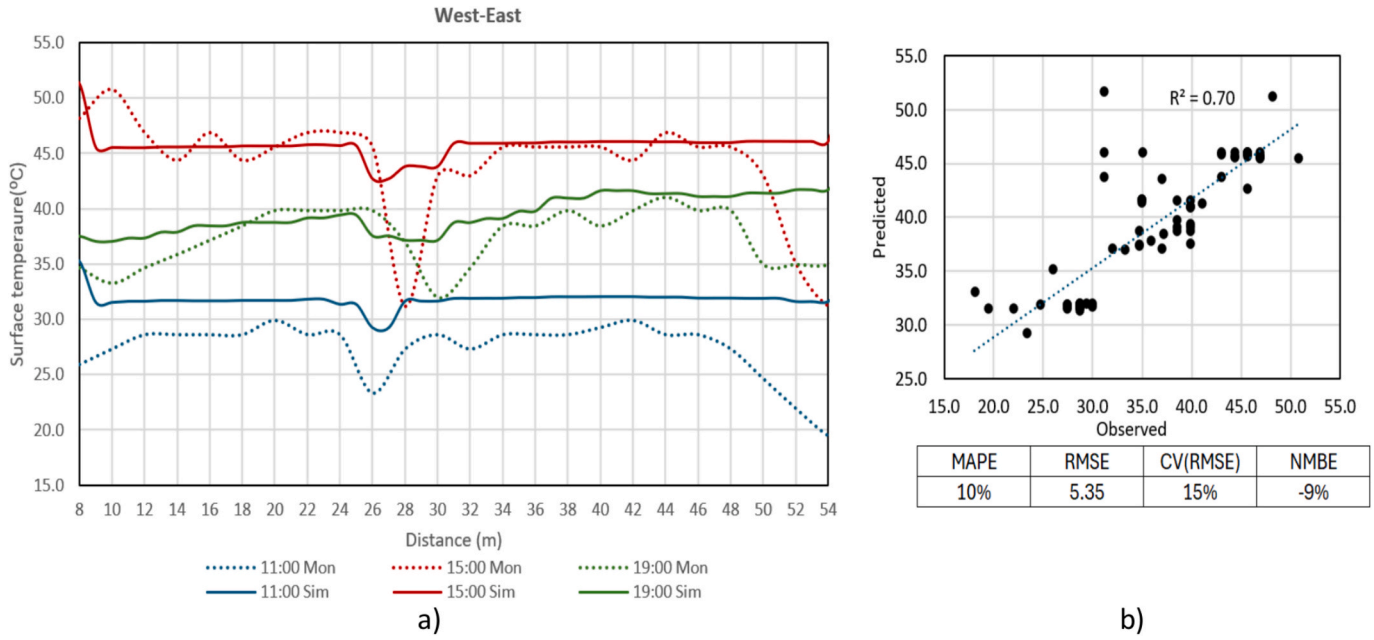

Fig. 7. a) Simulation and monitoring floor surface results in a west-east profile. b) regression analysis and statistical error parameter results.

the square. The simulation results were able to reproduce the changes in the surface temperature under the shade accurately. The calculation of statistical error provided a R^2 of 0.7, a RMSE of 5.28 °C, MAPE of 10 %, a cvRMSE of 14.7 % and a nMBE of − 6.9 % considering all data.

3.2. Longwave MRT results

Fig. 9 shows the calculated longwave mean radiant temperature from thermography and simulated results at 1.5 m above the ground of the 20 points at the three hours of the analysis. The mean values of monitored LW MRT were 21.5 °C, 29.1 °C, and 27.2 °C, while the simulated ones were 24.1 °C, 33.3 °C, and 29.9 °C. This shows that simulated temperatures were generally higher at all hours, although the difference was higher in the afternoon hours and lower in the morning and evening. The spatial variation of LW MRT values among points was different too. While simulated data provided lower results from east to west (1 to 5), the calculated results tended to produce higher values in the middle points (2). Comparing results from north to south (A to D), calculated values provided higher values in the middle points (B and C), while simulated ones provided more similar values in this direction, with a slight tendency to be higher in the north part (A values).

The calculation of statistical error considering all data provided a R^2 of 0.9, MAPE of 12.3 %, a RMSE of 3.4 °C, a cvRMSE of 13.2 %, and a nMBE of − 12.2 %.

3.3. MRT results

The simulation model was used to predict the MRT (including shortwave and longwave MRT) and it was compared to the calculated MRT considering the longwave component obtained from aerial thermography and the shortwave component using the SDIM method. The results in each of the 20 analyzed points at the three hours of the day are shown in Fig. 10. The mean values of monitored MRT were 55.2 °C, 70.2 °C, and 52.1 °C at 11:00, 15:00, and 19:00 h respectively, while the simulated ones were 57.4 °C, 71.0 °C, and 53.2 °C. The simulated mean values are higher than the monitored ones. However, analyzing each point, there are many of them that show greater values of monitoring than simulations, especially those points that are under the direct sun. The effect of direct sun on MRT increases the spatial variability of the results. Once including the shortwave radiation influence on MRT, the spatial variation on MRT achieved differences up to 30 °C.

The calculation of statistical error considering all data provided an R^2 of 0.93, MAPE of 6.0 %, an RMSE of 4.2 °C, a cvRMSE of 7.1 %, and an nMBE of − 2.3 %.

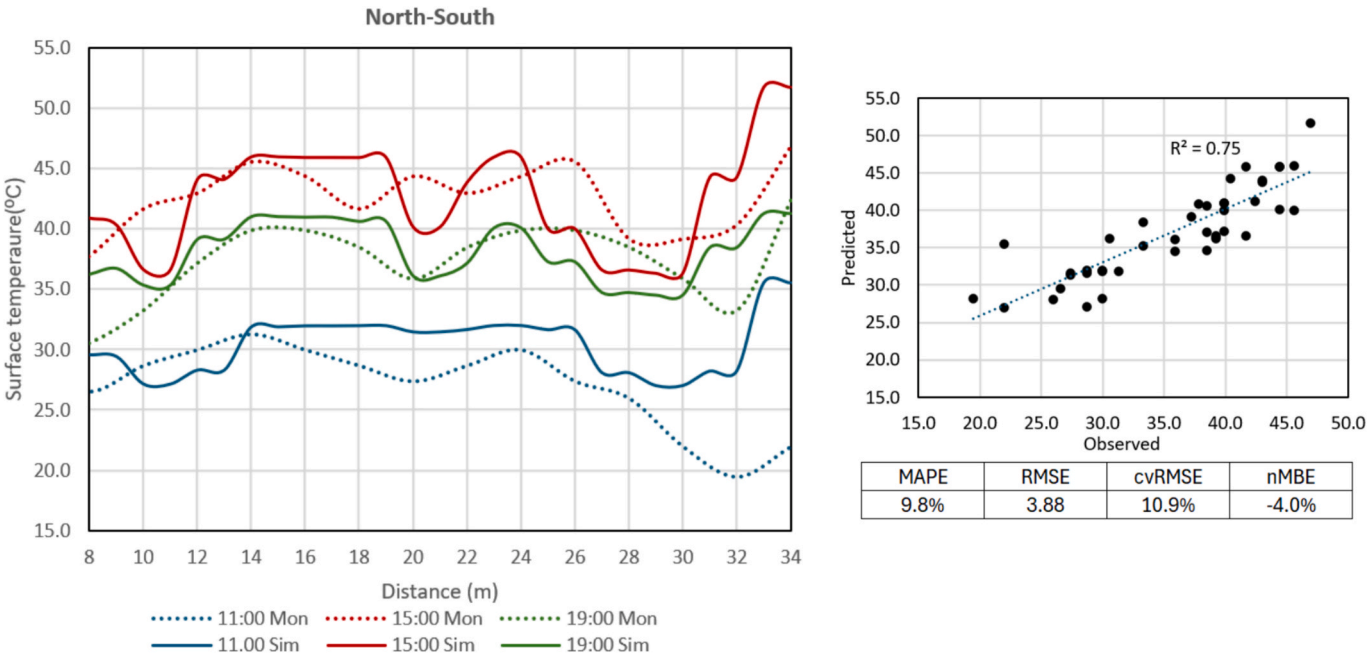

MAPE	RMSE	cvRMSE	nMBE
9.8%	3.88	10.9%	-4.0%

Fig. 8. a) Simulation and monitoring floor surface results in a north-south profile. b) regression analysis and statistical error parameter results.

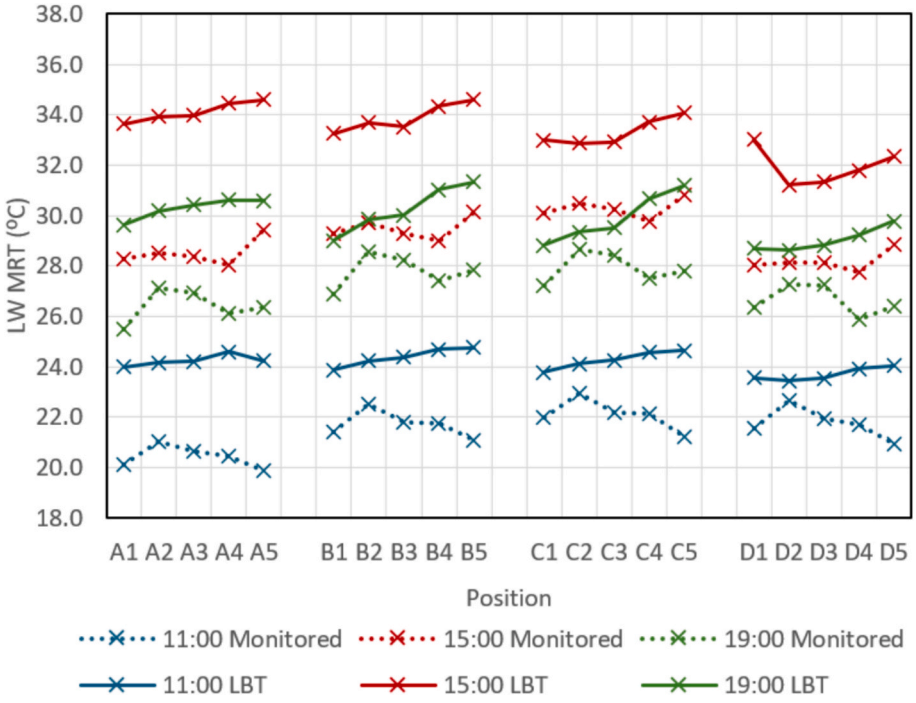

Fig. 9. Simulated and calculated LW MRT at 1.5 m at the selected hours and points.

3.4. Comfort results

The LBT simulation script used allows for the calculation of the comfort parameter UTCI. The potential of the simulation allows extracting comfort maps at different times, as shown in Fig. 11, for the studied day. These maps show the direct relationship between MRT and UTCI, as the UTCI map clearly shows important differences between shaded and exposed areas during the day. In the night, the UTCI values are more homogeneous in the square. Maximum values of UTCI were obtained at 16:00 h, with 38 °C in solar-exposed areas, and minimum values were obtained during the night, with 16 °C at 3.00 h.

4. Discussion

This study proposed a calibration methodology for urban MRT simulations using Ladybug Tools® (LBT) and aerial thermography, aiming to improve thermal comfort simulations in urban settings. The findings show that simulated longwave MRT aligns well with monitoring data, despite some discrepancies that highlight model limitations. These results underscore both the potential and constraints of aerial thermography as a validation tool for thermal simulations.

The comparison between monitored and simulated surface temperature data allowed for model calibration, primarily by adjusting

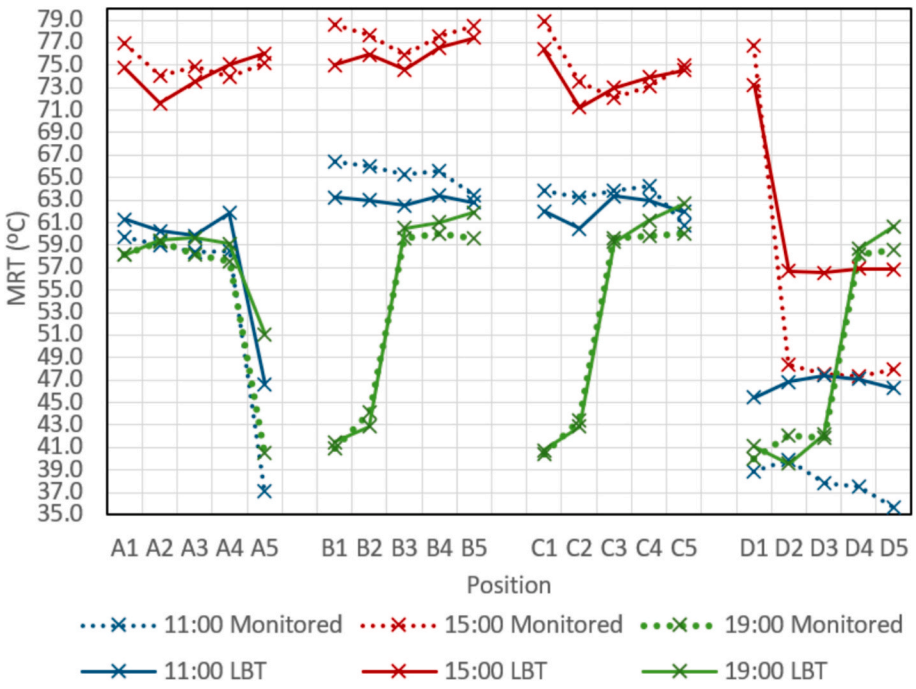

Fig. 10. MRT results from simulation and calculation methods.

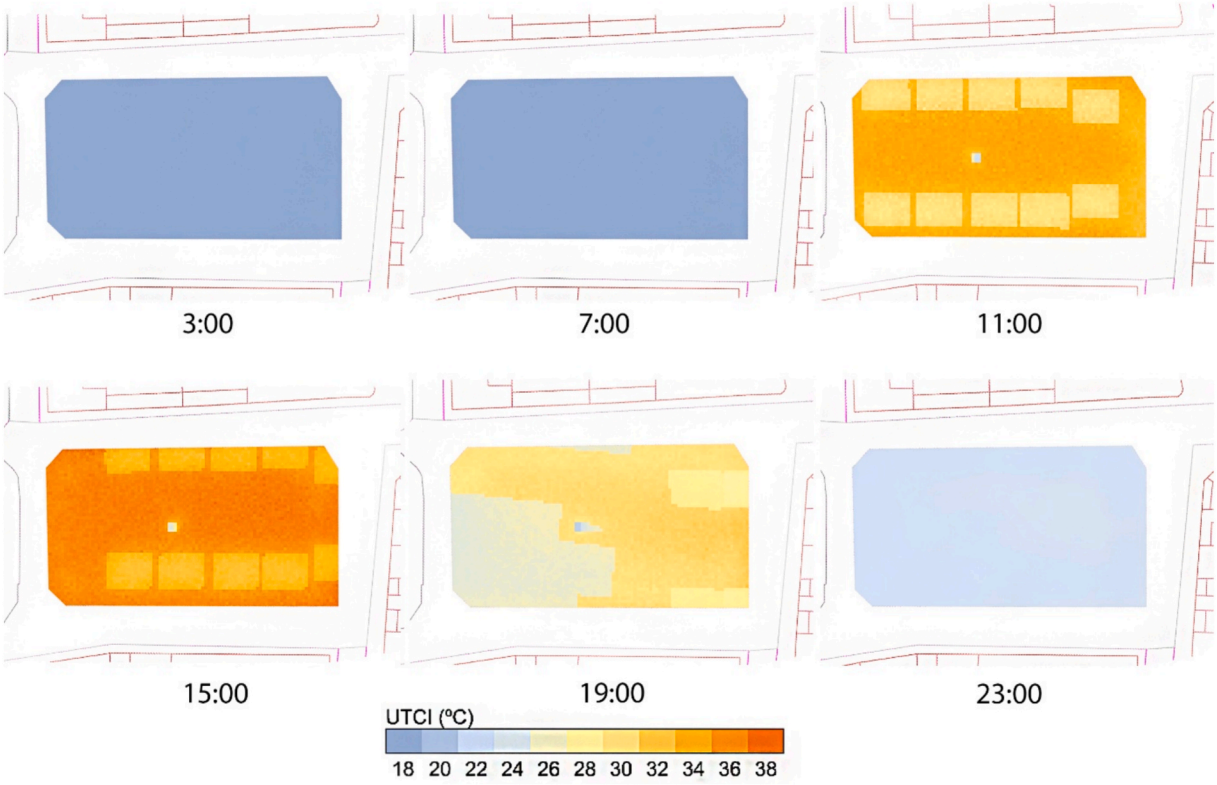

Fig. 11. Thermal comfort maps (UTCI) from LBT at different times on the 20th of July 2021.

material properties and ground geometry. Aerial thermography, which directly captures surface temperature, served as the basis for these adjustments. Model calibration is extremely important, as previously demonstrated by other studies like Schoneberger et al [13], where albedo calibration coupled with cloud cover calibration reduced model RMSE from 10.17 K to 5.07 K. Other studies without calibration found RMSE higher than 10 °C in MRT simulated with SOLWEIG, Rayman and ENVI-met [34]. In our case, with clear skies, albedo emerged as the property with the greatest influence on surface temperature, as suggested by previous research [56], where the authors estimated about a 4–5 °C change in MRT values per increase of 0.1 in albedo in the central hours of the day. Other parameters, like the grid resolution for subdividing the model ground surface, significantly affected result variations across profile lines. Additionally, shading properties (e.g.,

transmittance) required correction to align simulated results with monitored data under vegetation shade. However, the simplistic representation of vegetation in LBT, which lacks evapotranspiration effects and assumes air-temperature equivalence, likely contributed to inaccuracies. Post-calibration metrics, shown in Fig. 7b and Fig. 8b, were within ASHRAE Guidelines, except for the R^2 of 0.7. However, considering that only three hours of monitored data were used and the simulation software limitations, these values are considered acceptable.

For longwave MRT, the simulation results shown in section 4.2 (Fig. 9) were generally higher than monitored values. While R^2 (0.90) and cvRMSE (13.2 %) met ASHRAE thresholds, nMBE (−12.2 %) exceeded them slightly. These results differ from previous studies [40], which reported LBT underestimating longwave MRT when compared to pyrgeometer measurements. This discrepancy may stem from differences in experimental settings, as the referenced study focused exclusively on shaded areas. In the present study, the largest differences occurred in the afternoon (15:00 h), with no clear correlation to shading or exposure, suggesting that other factors, such as diffuse radiation, may influence the deviations. Directly related to diffuse radiation is vegetation, and the way LBT models the vegetation can be the reason for inaccuracies. Previous studies analyzing longwave radiation simulation with other software, in this case ENVI-met, also found an overestimation of simulated longwave radiation in shaded areas [13]. In contrast, simulations with the SOLWEIG model showed underestimation of longwave radiation [57].

Overall, MRT results shown in Fig. 10 showed better alignment between simulation and monitoring, with an R^2 of 0.93, a cvRMSE of 7.1 %, and an nMBE of − 2.3 %, all well within ASHRAE thresholds. In addition, the Mean Absolute Error of 2.9 °C is within the ± 5 °C accuracy recommended by ISO 7726 for MRT under thermal stress conditions, considering this standard as a benchmark. These results have important implications. First, the higher simulated longwave MRT is offset by the shortwave MRT, resulting in a global MRT closer to the values derived from monitored data. This observation is crucial for interpreting the software's application. Second, the SDIM method, used to calculate MRT from monitoring data and validated by prior studies [47], produces results closely matching those of the ray-tracing method employed by Radiance in the LBT simulation. This suggests that the shortwave MRT component in LBT may be underestimated, though the overall MRT compensates for this discrepancy. The accuracy of the results provided by the LBT simulation of MRT falls within the range reported by previous works that compared in situ measurements with widely used models. For instance, [57] compared net radiometer measurements against SOLWEIG simulations, obtaining R2 values higher than 0.9, although with an average overestimation of 4 °C, attributed to overestimated lateral longwave radiant fluxes. This bias is consistent with the slight discrepancies observed in our study under certain geometric conditions. For ENVI-met, [13] demonstrated a consistent MRT overestimations, achieving RMSE = 5.07 °C in open spaces and RMSE = 1.5 °C in shaded areas.

It is interesting to analyze differences in accuracy between shaded and sunny areas, as the previous reference study proposed. To do so, Table 4 has been included, showing the difference between monitoring and simulation at every point analyzed, in both MRT and LW MRT results (extracted from Fig. 9 and Fig. 10). When analyzing points without direct solar radiation (marked in bold in Table 4), the difference between simulated and monitored MRT is greatest, particularly at 11:00 and 15:00. These trends do not correlate with differences in longwave MRT for the same points, indicating that the deviation likely stems from another factor, possibly the diffuse radiation component. In our study, shaded areas were primarily provided by vegetation, suggesting that the transparency and material properties assigned to vegetation in LBT require further calibration to enhance accuracy. Addressing this limitation represents an important avenue for future research.

Considering only the values in sunny points, the RMSE is 2.4°C, 1.8°C lower than the global RMSE of 4.2 °C when considering all points.

Table 4
Difference between simulation and monitoring derived results of MRT and LW MRT. The numbers in bold are points in the shade.

	MRT			LW MRT		
Point	**11:00**	**15:00**	**19:00**	**11:00**	**15:00**	**19:00**
A1	− 1.6	2.2	0.0	− 3.9	− 5.4	− 4.2
A2	− 1.3	2.5	− 0.1	− 3.1	− 5.4	− 3.0
A3	− 1.4	1.3	− 1.4	− 3.6	− 5.6	− 3.5
A4	− 3.4	− 1.1	− 1.6	− 4.1	− 6.4	− 4.5
A5	**− 9.6**	− 0.9	**− 10.6**	**− 4.3**	− 5.2	**− 4.2**
B1	3.2	3.5	**− 0.5**	− 2.5	− 4.0	**− 2.1**
B2	3.0	1.8	**1.2**	− 1.7	− 4.0	**− 1.3**
B3	2.7	1.3	− 1.0	− 2.6	− 4.2	− 1.8
B4	2.2	1.0	− 1.0	− 2.9	− 5.4	− 3.6
B5	0.7	1.1	− 2.2	− 3.7	− 4.4	− 3.5
C1	1.8	2.5	**− 0.4**	− 1.8	− 2.9	**− 1.6**
C2	2.8	2.3	**0.6**	− 1.2	− 2.4	**− 0.7**
C3	0.5	− 0.9	0.3	− 2.1	− 2.7	− 1.1
C4	1.3	− 0.8	− 1.3	− 2.4	− 4.0	− 3.2
C5	− 1.2	0.4	− 2.7	− 3.4	− 3.3	− 3.4
D1	**− 6.6**	3.4	**− 1.1**	**− 2.0**	− 5.0	**− 2.3**
D2	**− 7.0**	**− 8.3**	**2.5**	**− 0.8**	**− 3.0**	**− 1.4**
D3	**− 9.5**	**− 9.0**	**− 0.3**	**− 1.6**	**− 3.2**	**− 1.6**
D4	**− 9.5**	**− 9.5**	−0.5	**− 2.2**	**− 4.1**	− 3.3
D5	**− 10.7**	**− 8.9**	−2.0	**− 3.1**	**− 3.5**	− 3.4

These findings suggest that although the simulated MRT is validated, users should still consider the overestimation of MRT in shaded areas. In addition, further analysis should be conducted in order to validate MRT results at other times of the day, when there is no direct solar radiation, especially during the night.

The applications of the LBT to analyze thermal comfort have been shown, and the UTCI in the square of the monitored day was simulated (Fig. 11). LBT is a versatile software that allows for the adjustments of model geometry and properties, and direct feedback of the results on the same modeling software, Rhinoceros. Hourly results are produced on spatial maps or specific points. This makes it a perfect tool for early design stages, but also for optimizing mitigation strategies. However, calibration of the models is a step that is not always easy to perform. With this new methodology using aerial thermography proposed in this study, one major outdoor simulation handicap is overcome. The findings of this study support and extend existing theory on the importance of MRT as a key driver of outdoor thermal comfort, particularly in climates characterized by high solar radiation and low wind speed.

By integrating aerial thermography with a structured calibration process, this study demonstrates a replicable method to enhance the accuracy of MRT simulations using Ladybug Tools®, a platform increasingly adopted in design practice but still under-validated. This contributes to bridging the gap between theoretical comfort modelling and its practical application in urban planning. The method provides a scalable and non-invasive approach for improving comfort assessment in real urban contexts, especially where instrument-based validation is not feasible. Regarding alternative measurement techniques, [19] developed a portable spherical thermography system based on infrared cameras and a rotating platform, obtaining differences within 1.6 °C compared to pyrgeometer measurements in six directions. While this method achieved high accuracy, it covered more limited areas than our UAV-based approach, which can capture extensive urban surfaces in a single flight. In a similar UAV context, [58] used drones equipped with multispectral and thermal cameras and validated results with globe thermometers. However, globe thermometers do not differentiate between shortwave and longwave components of MRT, whereas our approach explicitly validates the longwave component estimated from simulations.

This study introduces a novel approach by leveraging aerial thermography for the validation of MRT simulations, marking a significant advancement in this field. By addressing existing validation gaps, particularly in early-stage design tools like Ladybug Tools®, this

research enhances the reliability of these tools for urban thermal comfort assessments. The innovative methodology not only strengthens confidence in simulation outputs but also provides a practical framework for integrating robust calibration processes into urban planning workflows. It can be used to calibrate any other simulation software. The findings of this study are therefore significant both theoretically, by reinforcing the central role of MRT, and methodologically, by offering a new pathway to improve simulation reliability in early-stage urban design workflows.

Despite its strengths, this approach has certain limitations. Aerial thermography, while effective for capturing surface temperatures, cannot measure under-vegetation conditions or directly assess the shortwave MRT component, which relies on weather station data. Furthermore, strict aerial flight regulations require thoughtful preparation of the monitoring campaigns and careful design of the experiments. On the other hand, the simplifications and assumptions inherent in simulation models may not fully capture the complexity of real-world conditions, leading to discrepancies between simulated and observed results. The difference between simulation and calculated data shows that the setup of the model is critical. Small differences in material properties, especially albedo, produce an important variation in the results. This limitation could be overcome with more detailed data of the model and more precise modelling, although this would extend the simulation time. Additionally, vegetation modeling in LBT is overly simplistic, neglecting key factors like evapotranspiration and temperature variations, which may explain inaccuracies in shaded areas. Another factor to improve accuracy would be the validation with more hours of thermography. Given that in this test only one day of monitored data was available, the simulation was limited to that day. However, hourly simulations would be more accurate with longer monitored data.

5. Conclusion

This study presents a novel methodology for calibrating and validating outdoor longwave mean radiant temperature simulations using aerial thermography combined with meteorological data, providing a robust framework to enhance the accuracy of thermal comfort assessments across various simulation platforms. The calibration process refines key parameters, such as albedo, shading, and grid resolution, ensuring results align with ASHRAE guidelines. By validating the methodology through precise comparisons between simulated and monitored MRT, the study highlights its reliability and adaptability to various urban contexts, directly addressing the gap in the literature regarding MRT simulation validation, and offering a cost-effective, versatile alternative to existing methods.

Although Ladybug Tools® was used as the demonstration platform, the approach is broadly applicable to other simulation tools, providing urban planners with a practical method for refining early-stage thermal comfort evaluations. The results revealed that longwave MRT overestimation (RMSE = 3.4 °C) was offset by shortwave contributions, leading to total MRT values closely aligned with the monitored data, particularly for sun-exposed points (RMSE = 2.4 °C). The largest differences occurred in points under vegetation shade, suggesting diffuse shortwave deviations and emphasizing the limitation of vegetation modelling in this software. Nevertheless, the validation of LBT simulations within ASHRAE guideline thresholds confirms the robustness of the proposed workflow.

The study contributes to the limited but growing body of research on the validation of MRT simulations in outdoor urban spaces, providing a practical, cost-effective, and useful method that allows spatial validation using UAV-based thermography. By enhancing the reliability of MRT predictions it also lays the foundation for more robust thermal comfort assessments based on indices such as UTCI or PET. Future research should incorporate in situ shortwave radiation measurements and nighttime monitoring to further enhance the calibration process, particularly regarding material properties like thermal inertia. These improvements are essential for accurately simulating nighttime thermal comfort, a critical period for understanding the urban heat island effect and its mitigation in cities.

Overall, this methodology represents a significant step forward in urban thermal comfort modeling, offering a flexible and replicable tool for the design of thermally comfortable and sustainable urban environments. Its practical applications extend to smart city initiatives, where it can be coupled with monitoring systems for dynamic adaptation (such as automated shading), as well as to retrofitting strategies that optimize vegetation, surface materials, and urban geometry. By combining high-resolution remote sensing with open-source simulation, this approach provides urban planners with a scalable and precise method to enhance thermal resilience, reduce energy demand, and support climate change mitigation in contemporary and historical cities alike.

CRediT authorship contribution statement

V.P. Lopez-Cabeza: Writing – original draft, Visualization, Validation, Software, Methodology, Investigation, Formal analysis, Conceptualization. **M. Videras-Rodriguez:** Writing – review & editing, Software, Investigation, Data curation, Conceptualization. **S. Gomez-Melgar:** Writing – review & editing, Supervision, Resources, Methodology, Formal analysis. **J.M. Andujar-Marquez:** Writing – review & editing, Supervision, Resources, Project administration, Conceptualization.

Funding

This work is funded by grant JDC2023-050880-I funded by MICIU/AEI /10.13039/501100011033 and by ESF+, and by project PID2023-146213OA-I00 funded by MCIN/AEI/ https://doi.org/10.13039/501100011033 and by "ERDF A way of making Europe".

Declaration of competing interest

The authors declare that they have no known competing financial interests or personal relationships that could have appeared to influence the work reported in this paper.

Data availability

Data will be made available on request.

References

[1] Kim SW, Brown RD. Urban heat island (UHI) intensity and magnitude estimations: a systematic literature review. Sci Total Environ 2021;779:146389. https://doi.org/10.1016/j.scitotenv.2021.146389.
[2] Taleghani M. Outdoor thermal comfort by different heat mitigation strategies- a review. Renew Sustain Energy Rev 2018;81:2011–8. https://doi.org/10.1016/j.rser.2017.06.010.
[3] Nikolopoulou M. Outdoor thermal comfort. Front Biosci 2011;S3:1552. https://doi.org/10.2741/245.
[4] Lam CKC, Pan H, Nie W, Li X, Wu J, Yin Z, et al. Effects of perceived environmental quality and psychological status on outdoor thermal comfort: a panel study in Southern China. Sustain Cities Soc 2024;112:105578. https://doi.org/10.1016/J.SCS.2024.105578.
[5] Fiala D, Havenith G, Bröde P, Kampmann B, Jendritzky G. UTCI-Fiala multi-node model of human heat transfer and temperature regulation. Int J Biometeorol 2012;56:429–41. https://doi.org/10.1007/s00484-011-0424-7.
[6] Höppe P. The physiological equivalent temperature - a universal index for the biometeorological assessment of the thermal environment. Int J Biometeorol 1999;43:71–5. https://doi.org/10.1007/s004840050118.
[7] Kumar P, Sharma A. Study on importance, procedure, and scope of outdoor thermal comfort –a review. Sustain Cities Soc 2020;61:102297. https://doi.org/10.1016/j.scs.2020.102297.
[8] Lee H, Holst J, Mayer H. Modification of human-biometeorologically significant radiant flux densities by shading as local method to mitigate heat stress in summer within urban street canyons. Adv Meteorol 2013;2013:1–13. https://doi.org/10.1155/2013/312572.

[9] Kántor N, Unger J. The most problematic variable in the course of human-biometeorological comfort assessment - the mean radiant temperature. Central Eur J Geosci 2011;3:90–100. https://doi.org/10.2478/S13533-011-0010-X/MACHINEREADABLECITATION/RIS.

[10] Staiger H, Matzarakis A. Accuracy of mean radiant temperature derived from active and passive radiometry. Atmosphere 2020, Vol 11, Page 805 2020;11:805. 10.3390/ATMOS11080805.

[11] Colaninno N, Salvati A, Lopez J, Morganti M. District-scale cumulative heat stress mapping using very-high-resolution spatiotemporal simulation. Sustain Cities Soc 2025:106498. 10.1016/J.SCS.2025.106498.

[12] Lopez-Ordoñez C, Garcia-Nevado E, Coch H, Morganti M. Heat stress in social housing districts: tree cover–built form interaction. Build Cities 2025;6:415–32. https://doi.org/10.5334/BC.598.

[13] Schöneberger P, Sinsel T, Ouyang W, Tan Z, Bruse M, Simon H. Enhancing urban microclimate simulations: validating ENVI-met's accuracy in modeling multi-directional radiative fluxes and mean radiant temperature in subtropical hong kong. Build Environ 2025;284:113475. https://doi.org/10.1016/J.BUILDENV.2025.113475.

[14] Guo H, Aviv D, Loyola M, Teitelbaum E, Houchois N, Meggers F. On the understanding of the mean radiant temperature within both the indoor and outdoor environment, a critical review. Renew Sustain Energy Rev 2020;117:109207. https://doi.org/10.1016/j.rser.2019.06.014.

[15] Thorsson S, Lindberg F, Eliasson I, Holmer B. Different methods for estimating the mean radiant temperature in an outdoor urban setting. Int J Climatol 2007;27:1983–93. https://doi.org/10.1002/joc.1537.

[16] Banfi A, Tatti A, Ferrando M, Fustinoni D, Zanghirella F, Causone F. An experimental technique based on globe thermometers for the measurement of mean radiant temperature in urban settings. Build Environ 2022;222:109373. https://doi.org/10.1016/J.BUILDENV.2022.109373.

[17] Li Z, Feng X, Fang Z. A modified method to measure outdoor mean radiant temperature: Comparison between two-hemisphere method and six-direction integral method. Build Environ 2022;221:109292. https://doi.org/10.1016/J.BUILDENV.2022.109292.

[18] Johansson E, Thorsson S, Emmanuel R, Krüger E. Instruments and methods in outdoor thermal comfort studies - the need for standardization. Urban Clim 2014;10:346–66. https://doi.org/10.1016/j.uclim.2013.12.002.

[19] Asawa T, Oshio H, Tanaka K. Portable recording system for spherical thermography and its application to longwave mean radiant temperature estimation. Build Environ 2022;222:109412. https://doi.org/10.1016/j.buildenv.2022.109412.

[20] Prades-Gil C, Viana-Fons JD, Masip X, Cazorla-Marín A, Gómez-Navarro T. Methodology to assess the impact of urban vegetation on the energy consumption of residential buildings. Case study in a Mediterranean city. Energy Convers Manage: X 2024;24:100706. https://doi.org/10.1016/J.ECMX.2024.100706.

[21] Rodríguez MV, Melgar SG, Márquez JMA. Assessment of aerial thermography as a method of in situ measurement of radiant heat transfer in urban public spaces. Sustain Cities Soc 2022;87:104228. https://doi.org/10.1016/J.SCS.2022.104228.

[22] Rodríguez MV, Melgar SG, Cordero AS, Márquez JMA. A critical review of unmanned aerial vehicles (UAVs) use in architecture and urbanism: scientometric and bibliometric analysis. Appl Sci 2021, vol 11, Page 9966 2021;11:9966. 10.3390/APP11219966.

[23] Song B, Park K. Verification of accuracy of unmanned aerial vehicle (UAV) land surface temperature images using in-situ data. Remote Sens 2020, Vol 12, Page 288 2020;12:288. 10.3390/RS12020288.

[24] Lee DS, Kim EJ, Cho YH, Kang JW, Jo JH. A field study on application of infrared thermography for estimating mean radiant temperatures in large stadiums. Energ Buildings 2019;202:109360. https://doi.org/10.1016/J.ENBUILD.2019.109360.

[25] Zhao X, Luo Y, He J. Analysis of the thermal environment in pedestrian space using 3D thermal imaging. Energies 2020;13:3674. 10.3390/EN13143674.

[26] Roy TB, Middey A, Krupadam RJ. Unveiling the microclimate: a comprehensive review of tools, techniques, and future directions for sustainable cities. Build Environ 2025;274:112726. https://doi.org/10.1016/J.BUILDENV.2025.112726.

[27] Tsoka S, Tsikaloudaki A, Theodosiou T. Analyzing the ENVI-met microclimate model's performance and assessing cool materials and urban vegetation applications–a review. Sustain Cities Soc 2018;43:55–76. https://doi.org/10.1016/j.scs.2018.08.009.

[28] Aleksandrowicz O, Saroglou T, Pearlmutter D. Evaluation of summer mean radiant temperature simulation in ENVI-met in a hot Mediterranean climate. Build Environ 2023;245:110881. https://doi.org/10.1016/J.BUILDENV.2023.110881.

[29] Mao J. Automatic calibration of an urban microclimate model under uncertainty. Massachusetts Institute of Technology 2018.

[30] (ed) Schlünzen KH, (ed) Sokhi RS. Overview of tools and methods for meteorological and air pollution mesoscale model evaluation and user training. 2008.

[31] ENVI-met n.d. https://www.envi-met.com/ (accessed October 28, 2019).

[32] Matzarakis A, Rutz F, Mayer H. Modelling radiation fluxes in simple and complex environments: basics of the RayMan model. Int J Biometeorol 2010;54:131–9. https://doi.org/10.1007/s00484-009-0261-0.

[33] Lindberg F, Holmer B, Thorsson S. SOLWEIG 1.0 – Modelling spatial variations of 3D radiant fluxes and mean radiant temperature in complex urban settings. Int J Biometeorol 2008;52:697–713. https://doi.org/10.1007/s00484-008-0162-7.

[34] Du J, Sun C, Liu L, Chen X, Liu J. Comparison and modification of measurement and simulation techniques for estimating Tmrt in summer and winter in a severely cold region. Build Environ 2021;199:107918. https://doi.org/10.1016/j.buildenv.2021.107918.

[35] Mauree D, Naboni E, Coccolo S, Perera ATD, Nik VM, Scartezzini J-L. A review of assessment methods for the urban environment and its energy sustainability to guarantee climate adaptation of future cities. Renew Sustain Energy Rev 2019;112:733–46. https://doi.org/10.1016/J.RSER.2019.06.005.

[36] Ladybug Tools | Home Page n.d. https://www.ladybug.tools/ (accessed March 13, 2024).

[37] López-Cabeza VP, Diz-Mellado E, Rivera-Gómez C, Galán-Marín C, Samuelson HW. Thermal comfort modelling and empirical validation of predicted air temperature in hot-summer Mediterranean courtyards. J Build Perform Simul 2022;15:39–61. https://doi.org/10.1080/19401493.2021.2001571.

[38] Elwy I, Ibrahim Y, Fahmy M, Mahdy M. Outdoor microclimatic validation for hybrid simulation workflow in hot arid climates against ENVI-met and field measurements. Energy Procedia 2018. https://doi.org/10.1016/j.egypro.2018.10.009.

[39] Evola G, Costanzo V, Magrì C, Margani G, Marletta L, Naboni E. A novel comprehensive workflow for modelling outdoor thermal comfort and energy demand in urban canyons: results and critical issues. Energ Buildings 2020;216:109946. https://doi.org/10.1016/j.enbuild.2020.109946.

[40] Nicholson S, Nikolopoulou M, Watkins R, Löve M, Ratti C. Data driven design for urban street shading: validation and application of ladybug tools as a design tool for outdoor thermal comfort. Urban Clim 2024;56:102041. https://doi.org/10.1016/J.UCLIM.2024.102041.

[41] Rodriguez MV, Melgar SG, Marquez JMA. Design recommendations for the rehabilitation of an urban canyon in a subtropical climate region using aerial thermography and simulation tools. Energ Buildings 2023;298:113525. https://doi.org/10.1016/J.ENBUILD.2023.113525.

[42] ASHRAE. ASHRAE guideline 14-2014. Measurement of energy, demand, and water savings; 2014.

[43] Kottek M, Grieser J, Christoph Beck Fr. BR. World map of the Köppen-Geiger climate classification updated. Sustain Build Climate Initiative 2009;15:62. https://doi.org/10.1127/0941-2948/2006/0130.

[44] Höppe P. A new procedure to determine the mean radiant temperature outdoors. Wetter Unt Leben 1992;44:147–51.

[45] Cohen S, Palatchi Y, Palatchi DP, Shashua-Bar L, Lukyanov V, Yaakov Y, et al. Mean radiant temperature in urban canyons from solar calculations, climate and surface properties – Theory, validation and 'Mr.T' software. Build Environ 2020;178:106927. https://doi.org/10.1016/J.BUILDENV.2020.106927.

[46] Campbell GS, Norman JM. An introduction to environmental biophysics. Springer Science & Business Media; 2000.

[47] Krüger EL, Minella FO, Matzarakis A. Comparison of different methods of estimating the mean radiant temperature in outdoor thermal comfort studies. Int J Biometeorol 2014;58:1727–37. https://doi.org/10.1007/S00484-013-0777-1/METRICS.

[48] Sadeghipour Roudsari M, Pak M, Smith A. Ladybug: a parametric environmental plugin for grasshopper to help designers create an environmentally-conscious design. In: 13th Conference of International Building Performance Simulation Association; 2013. p. 3129–35.

[49] EnergyPlus Engineering Reference 2021.

[50] Radiance — Radsite n.d. https://www.radiance-online.org/ (accessed December 23, 2024).

[51] UTCI Comfort Map | HB-Energy Primer n.d. https://docs.ladybug.tools/hb-energy-primer/components/7_thermalmap/utci_comfort_map (accessed March 13, 2024).

[52] Arens E, Hoyt T, Zhou X, Huang L, Zhang H, Schiavon S. Modeling the comfort effects of short-wave solar radiation indoors. Build Environ 2015;88:3–9. https://doi.org/10.1016/J.BUILDENV.2014.09.004.

[53] Climate.OneBuilding.Org n.d. http://climate.onebuilding.org/ (accessed September 15, 2021).

[54] Armstrong JS, Collopy F. Error measures for generalizing about forecasting methods: empirical comparisons. Int J Forecast 1992;8:69–80. https://doi.org/10.1016/0169-2070(92)90008-W.

[55] Willmott CJ. Some comments on the evaluation of model performance. Bull Am Meteorol Soc 1982;63:1309–13. https://doi.org/10.1175/1520-0477(1982)063<1309:SCOTEO>2.0.CO;2.

[56] Elmagri H, Kamel TM, Ozer H. Assessment of the effectiveness of cool pavements on outdoor thermal environment in urban areas. Build Environ 2024;266:112095. https://doi.org/10.1016/J.BUILDENV.2024.112095.

[57] Chen L, Yu B, Yang F, Mayer H. Intra-urban differences of mean radiant temperature in different urban settings in Shanghai and implications for heat stress under heat waves: a GIS-based approach. Energ Buildings 2016;130:829–42. https://doi.org/10.1016/j.enbuild.2016.09.014.

[58] Rüdisser D, Weiss T, Unger L. Spatially resolved analysis of urban thermal environments based on a three-dimensional sampling algorithm and UAV-based radiometric measurements. Sensors 2021;21:4847. 10.3390/S21144847.